

# 1 Seasonal Prediction Skill of East Asian Summer Monsoon in CMIP5-Models

2 *Bo Huang,\* Ulrich Cubasch, Christopher Kadow*

3 *Institute of Meteorology, Freie Universität Berlin,*  
4 *Carl-Heinrich-Becker-Weg 6-10, 12165 Berlin, Germany*

5 *Email: huangb@zedat.fu-berlin.de*

## 6 7 **ABSTRACT**

8 The East Asian summer monsoon (EASM) is an important part of the global climate system  
9 and plays a vital role in the Asian climate. Its seasonal predictability is a long-standing issue  
10 within the monsoon scientist community. In this study, we will analyse the seasonal (the  
11 leading time is at least six months) prediction skill of the EASM rainfall and its associated  
12 general circulation in non-initialised and initialised simulations for the years 1979-2005  
13 which were performed by six prediction systems (*i.e.*, the BCC-CSM1-1, the CanCM4, the  
14 GFDL-CM2p1, the HadCM3, the MIROC5 and the MPI-ESM-LR) from the Coupled Model  
15 Intercomparison Project phase 5 (CMIP 5). We found that most prediction systems simulated  
16 zonal wind over 850 and 200 hPa were significantly improved in the initialised simulations  
17 compared to non-initialised simulations. Based on the knowledge that zonal wind indices can  
18 be used as potential predictors for the EASM, we selected an EASM index based upon the  
19 zonal wind over 850 hPa for further analysis. This assessment showed that the GFDL-CM2p1  
20 and the MIROC5 added prediction skill in simulating the EASM index with initialisation, the  
21 BCC-CSM1-1, the CanCM4, and the MPI-ESM-LR changed the skill insignificantly, and the  
22 HadCM3 indicated a decreased skill score. The different response to the initialisation can be  
23 traced back to the ability of the models to capture the ENSO (El Niño-Southern Oscillation)-  
24 EASM coupled mode, particularly the Southern Oscillation-EASM coupled mode. As it is  
25 known from observational studies, this mode links the oceanic circulation and the EASM  
26 rainfall. On the whole, we find that the GFDL-CM2p1 and the MIROC5 are capable of  
27 predicting the EASM on a seasonal time-scale under the current initialisation strategy.

28 **Key Words:** East Asian summer monsoon; initialisation; seasonal prediction; ENSO-EASM  
29 coupled mode; CMIP5

## 30 1. INTRODUCTION

31 The Asian monsoon is the most powerful monsoon system in the world due to the thermal  
32 contrast between the Eurasian continent and the Indo-Pacific Ocean. Its evolution and  
33 variability critically influences the livelihood and the socio-economic status of over two  
34 billion people who live in the Asian monsoon dominated region. It encompasses two sub-  
35 monsoon systems, the South Asian monsoon (SAM) and the East Asian monsoon (EAM)  
36 (Wang, 2006). In summer time (June-July-August), the EAM, namely, the East Asian  
37 summer monsoon (EASM) occurs from the Indo-China peninsula to the Korean Peninsula  
38 and Japan, and shows strong intraseasonal-to-interdecadal variability (Ding and Chan, 2005).  
39 Thus, an accurate prediction of the EASM is an important and long-standing issue in climate  
40 science.

41 To predict the EASM, there are two approaches, a statistical prediction and a dynamical  
42 prediction, respectively. The statistical method seeks the relationship between the EASM and  
43 a strong climate signal (e.g., ENSO, NAO; Wu et al., 2009;Yim et al., 2014;Wang et al.,  
44 2015). This method establishes an empirical equation between the EASM and climate index.  
45 However, it is limited by the strength of the climate signal. The other method is a dynamical  
46 prediction. It employs a climate model to predict the EASM (Sperber et al., 2001;Kang and  
47 Yoo, 2006;Wang et al., 2008a;Yang et al., 2008;Lee et al., 2010;Kim et al., 2012). Without  
48 initialisation, both the atmosphere general circulation models (AGCMs) and the coupled  
49 atmosphere-ocean general circulation models (CGCMs) cannot predict the climate on a  
50 seasonal time-scale (Goddard et al., 2001). Given an initial condition, the AGCMs have the  
51 ability to predict the climate, but show little skill in predicting the EASM (Wang et al.,  
52 2005;Barnston et al., 2010). Because the AGCMs fail to produce a correct relationship  
53 between the EASM and the sea surface temperature (SST), anomalies over the tropical  
54 western North Pacific, the South China Sea, and the Bay of Bengal (Wang et al., 2004;Wang  
55 et al., 2005). Therefore, the monsoon community endeavours to predict the EASM with  
56 CGCMs (Wang et al., 2008a;Zhou et al., 2009;Kim et al., 2012;Jiang et al., 2013).

57 CGCMs have proved to be the most valuable tools in predicting the EASM (Wang et  
58 al., 2008a;Zhou et al., 2009;Kim et al., 2012;Jiang et al., 2013). However, the performance of  
59 CGCMs in predicting the EASM on seasonal time-scale strongly depends on their ability to  
60 reproduce the air-sea coupled process (Kug et al., 2008) and the given initial condition (Wang  
61 et al., 2005). In the coupled model inter-comparison project (CMIP) phase 3 (CMIP3; Meehl

62 et al., 2007) era, the models simulate, not only a too weak tropical SST-monsoon  
63 teleconnection (Kim et al., 2008;Kim et al., 2011), but also a too weak East Asian zonal  
64 wind-rainfall teleconnection (Sperber et al., 2013). Compared to CMIP3 models, CMIP phase  
65 5 (CMIP5; Taylor et al., 2012) models improved the representation of monsoon status  
66 (Sperber et al., 2013). Therefore, given the initial conditions, the CMIP5 models do have the  
67 potential to predict the EASM.

68 As mentioned, initial conditions do play a vital factor in predicting the EASM on sub-  
69 seasonal to seasonal time-scale (Wang et al., 2005;Kang and Shukla, 2006). Under the  
70 current set up of initialisation, the CMIP5 models showed the ability to predict the SST  
71 variation index (*i.e.*, El Niño-Southern Oscillation-ENSO index) of up to 15 months in  
72 advance (Meehl and Teng, 2012;Meehl et al., 2014;Choi et al., 2016). This extended  
73 prediction skill of the ENSO suggests that the EASM can be predicted on a seasonal time-  
74 scale if the dynamical link between the ENSO and monsoon circulations is well represented  
75 in these models. Two scientific questions will be addressed in this study: 1. How realistic are  
76 the initialised CMIP5 models in representing the EASM? 2. Can the CMIP5 models capture  
77 the dynamical link between the ENSO and EASM?

78 In this paper, we will intercompare the influence of the initialisation on the capability of  
79 the CMIP5 model to capture the EASM and the ENSO-EASM teleconnections. The model  
80 simulations, comparison data and methods are introduced in Section 2. Section 3 describes  
81 the seasonal skill of the rainfall predictions and the prediction of the associated general  
82 circulation of the EASM. The mechanism causing the differential response of the models to  
83 the initialisation is presented in Section 4. The discussions are shown in Section 5. Section 6  
84 summarises the findings of this paper.

## 85 **2. MODELS, DATA AND METHODS**

### 86 **2.1 MODELS AND INITIALISATION**

87 In this study, we assessed six prediction systems from CMIP5 project (Table 1). The six  
88 prediction systems have performed a yearly initialisation (Meehl et al., 2014). Their  
89 simulations can be used in seasonal prediction study. There are two group of experiments,  
90 without initialisation (non-initialisation) and with initialisation, respectively. For non-  
91 initialised simulations, the models were forced by observed atmospheric composition changes  
92 (reflecting both anthropogenic and natural sources) and, for the first time, including the time-  
93 evolving land cover (Taylor et al., 2012). For initialised simulations, the models update the

94 time-evolving observed atmospheric and oceanic component (Taylor et al., 2012). Following  
95 the CMIP5 framework, the six models established their initialisation strategy, which are  
96 summarised in Table 2. More details about the initialisation strategy of each model can be  
97 found in the reference paper in Table 1. To simplify the comparison, we select the first lead  
98 year (up to 12 months) results for further analysis. The HadCM3-ff is the full-field initialised  
99 simulation, which employs the same CGCM (HadCM3) as the anomaly initialisation. We  
100 select the satellite era (1979 to 2005) for our study due to the spatial coverage of precipitation  
101 observations.

## 102 **2.2 COMPARISON DATA**

103 The main datasets which were used for comparison in this study include: (1) monthly  
104 precipitation data from the Global Precipitation Climatology Project (GPCP; Adler et al.,  
105 2003); (2) monthly circulation data from ECMWF Interim re-analysis (ERA-Interim; Dee et  
106 al., 2011); and (3) monthly mean SST from National Oceanic and Atmospheric  
107 Administration (NOAA) improved Extended Reconstructed SST version 4 (ERSST v4;  
108 Huang et al., 2015). All the model data and the comparison data are remapped onto a  
109 common grid of  $2.5^{\circ} \times 2.5^{\circ}$  by bi-linear interpolation to reduce the uncertainty induced by  
110 different data resolutions.

## 111 **2.3 EAST ASIAN MONSOON INDEX AND ENSO INDEX**

112 In recent decades, more than 25 general circulation indices have been produced to  
113 define the variability and the long-term change of the EASM. Wang et al. (2008b) arranged  
114 them according to their ability to capture the main features of the EASM. They found that the  
115 Wang and Fan index (hereafter WF-index; 1999) showed the best performance in capturing  
116 the total variance of the precipitation and three-dimensional circulation over East Asia. We,  
117 thus, select the WF-index for further analysis. Its definition is a standardised average zonal  
118 wind at 850 hPa in ( $5^{\circ}$ - $15^{\circ}$ N,  $90^{\circ}$ - $130^{\circ}$ E) minus in ( $22.5^{\circ}$ - $32.5^{\circ}$ N,  $110^{\circ}$ - $140^{\circ}$ E). The WF-  
119 index is a shear vorticity index which often is described by a north-south gradient of the zonal  
120 winds. In positive (negative) phase of the WF-index years, two strong (weak) rainfall belts  
121 located at the Indo China Peninsula-to-the Philippine Sea and the northern China-to-the  
122 Japanese Sea, and a weak (strong) rainfall belt occurs from the Yangtze river basin-to-the  
123 south of Japan. The June-July-August mean of WF-index is used to represent the EASM for  
124 further analysis in this study.

125 Here, we choose the Niño3.4 and southern oscillation index (SOI) to represents the  
 126 ENSO status. The Niño3.4 is calculated by the SST anomaly in the central Pacific (190-  
 127 240°E, 5°S-5°N), while the SOI is based upon the anomaly of the sea level pressure  
 128 differences between Tahiti (210.75°E, 17.6°S) and Darwin (130.83°E, 12.5°S). To calculate  
 129 the SOI, we interpolate the grid data to the Tahiti and the Darwin point by bilinear  
 130 interpolation.

#### 131 2.4 METHODS

132 In this study, we chose the un-centred Pattern Correlation Coefficient (PCC) (for more  
 133 details see Barnett and Schlesinger, 1987) to analyse the model performance in comparison to  
 134 the observational data, because centred correlations alone are not sufficient for the attribution  
 135 of seasonal prediction (Mitchell et al., 2001). The un-centred PCC is defined by:

$$PCC = \frac{\sum_{x=1}^n \sum_{y=1}^m w_{(x,y)} F_{(x,y)} A_{(x,y)}}{\sqrt{\sum_{x=1}^n \sum_{y=1}^m w_{(x,y)} F_{(x,y)}^2 \sum_{x=1}^n \sum_{y=1}^m w_{(x,y)} A_{(x,y)}^2}}$$

136

137 where n and m are grids on longitude and latitude, respectively.  $F_{(x,y)}$  and  $A_{(x,y)}$  represent two  
 138 dimensions comparison and validating value.  $w_{(x,y)}$  indicates the weighting coefficient for  
 139 each grid. An equal weighting coefficient was applied due to the study area in East Asia  
 140 where we can omit the convergence of the longitudes with the latitudes

141 We also employed the anomaly correlation coefficient (ACC) to analyse the model  
 142 performance in reproducing observational variations. The ACC is the correlation between  
 143 anomalies of forecasts and those of verifying values with the reference values, such as  
 144 climatological values (Drosowsky and Zhang, 2003). Its definition is:

$$ACC = \frac{\sum_{i=1}^n w_i (f_i - \bar{f})(a_i - \bar{a})}{\sqrt{\sum_{i=1}^n w_i (f_i - \bar{f})^2 \sum_{i=1}^n w_i (a_i - \bar{a})^2}}, (-1 \leq ACC \leq 1)$$

145

$$f_i = F_i - C_i, \bar{f} = \left( \sum_{i=1}^n w_i f_i \right) / \sum_{i=1}^n w_i$$

146

$$a_i = A_i - C_i, \bar{a} = \left( \sum_{i=1}^n w_i a_i \right) / \sum_{i=1}^n w_i$$

147

148 where  $n$  is the number of samples, and  $F_i$ ,  $A_i$ ,  $C_i$  represent comparison, verifying value,  
149 and reference value such as climatological value, respectively. Also,  $\bar{f}$  is the mean of  $f_i$ ,  $\bar{a}$  is  
150 the mean of  $a_i$ , and  $w_i$  indicates the weighting coefficient. If the variation of anomalies of  
151 comparison dataset is a coincident with that of the anomalies of verifying value, ACC will  
152 take 1 (the maximum value). Otherwise, if the variation is completely reversed, ACC is -1  
153 (the minimum value).

154 The root-mean-square-error (RMSE) is employed to check the model deviation from  
155 the observation and its definition is:

$$RMSE = \sqrt{\frac{\sum_{i=1}^n w_i D_i^2}{\sum_{i=1}^n w_i}}$$

156

157 where  $D_i$  represents the deviation between comparison and verifying value,  $w_i$  is the  
158 weighting coefficient for each sample, and  $n$  is the number of samples. If RMSE is closer to  
159 zero, it means that the comparisons are closer to the verifying values.

### 160 3. SEASONAL PREDICTION SKILL OF THE EASM

161 The EASM has complex spatial and temporal structures that encompass the tropics,  
162 subtropics, and midlatitudes (Tao and Chen, 1987;Ding, 1994). In the late spring, an  
163 enhanced rainfall pattern was observed in the Indochina Peninsula and in the South China  
164 Sea. At the same time, the rainfall belt advances northwards to the south of China. In the  
165 early summer, the rainfall concentration occurred in the Yangtze River Basin and in southern  
166 Japan, namely, the Meiyu and Baiu seasons, respectively. The rainfall belt can reach as far as  
167 northern China, the Korean Peninsula (called the Changma rainy season) and central Japan in  
168 July (Ding, 2004;Ding and Chan, 2005).

169 The EASM is characterised by both seasonal heterogeneous rainfall distribution and  
170 associated large-scale circulation systems (Wang et al., 2008b). In the summer season, water  
171 moisture migrates from the Pacific Ocean to central and eastern Asia, which is carried by the  
172 southwest surface winds. Generally, a strong summer monsoon year is followed by  
173 precipitation in northern China, while a weak summer monsoon year is usually accompanied  
174 by heavier rainfall along the Yangtze River basin (Ding, 1994;Zhou and Yu, 2005).

175 For multi-model ensemble mean (MME), the prediction skill of the June-July-August  
176 mean rainfall and the associated general circulation variable (*i.e.*, zonal and meridional wind,  
177 and mean sea level pressure) is presented in Figure 1. These variables have been widely used  
178 to calculate the monsoon index (Wang et al., 2008b). Table 3 shows the contribution of these  
179 variables in the EASM. Their abbreviations follow the guidelines of CMIP5 (Taylor et al.,  
180 2012). Compared to the non-initialised experiment, a larger predicted area can be found in the  
181 initialised experiment, especially for the psl, ua850 and ua200. There are small changes to the  
182 predicted area between the non-initialised and initialised experiment for the pr, va850 and  
183 va200. The individual model shows an acceptable performance (high PCC) in capturing the  
184 observed spatial variation of the six variables, but a poor performance in simulating their  
185 temporal variation (with low ACC) (Figure 2). There is no improvement in estimating the  
186 spatial variation of the six variables with initialisation. We can see that the models show a  
187 higher ACC in the initialised simulations than that in the non-initialised ones. The  
188 improvement of simulating the temporal variation of zonal winds (*i.e.*, ua850 and ua200) is  
189 larger than that of the rainfall and meridional winds. One can exploit this improvement by  
190 using a general circulation based monsoon index as a tool to predict the EASM. As  
191 mentioned in section 2.3, the WF-index better represents the monsoon rainfall and its  
192 associated general circulation structure than the other monsoon index. Therefore, the  
193 prediction skill of EASM in the following analysis is based on the WF-index.

194 In non-initialised simulations, none of the models captured the observed EASM, as  
195 indicated by an insignificant ACC (Figure 3). The CanCM4 and the GFDL-CM2p1 simulate  
196 a negative phase, while the BCC-CSM1-1, the HadCM3, the MIROC5 and the MPI-ESM-LR  
197 all predicted a positive phase of the EASM. With initialisation, the GFDL-CM2p1 and the  
198 MIROC5 improved the skill to simulate the EASM, the CanCM4 and the MPI-ESM-LR  
199 displayed hardly any reaction, while the BCC-CSM1-1 and the HadCM3 showed a worse  
200 performance than without initialisation. Particularly with anomaly initialisation, the HadCM3  
201 significantly lost its prediction skill in capturing the EASM. The CMIP5 models showed  
202 different response to the initialisation in predicting the EASM on seasonal time-scale. To  
203 understand the potential reason, we analysed the principle components of six variables, which  
204 contributed to the EASM. The details are presented in Section 4.

#### 205 4. EASM-ENSO COUPLED MODE IN CMIP5

206 We employed the EOF method to analyse the leading EOF modes of the six meteorological  
207 variables anomaly in the EASM region ( $0^{\circ}$ - $50^{\circ}$ N,  $100^{\circ}$ - $140^{\circ}$ E). The first EOF mode of the  
208 rainfall is characterised by a “sandwich” pattern, which showed sharp contrast between the  
209 prominent rainfall centre over Malaysia, the Yangtze River valley and the south of Japan, and  
210 the enhanced rainfall over the Indo-China Peninsula and the Philippine Sea (Figure 4). The  
211 increased precipitation is associated with cyclones in the low-level (850 hPa) and anti-  
212 cyclones in the upper level (200 hPa).

213 The correlation coefficient of the first eigenvector and the associated principal  
214 component (PC) between the model simulation and the observation in the non-initialised and  
215 the initialised simulation is presented in Figure 5. The models captured the eigenvector of the  
216 first EOF for the six meteorological fields in non-initialised simulation. However, they failed  
217 to reproduce the associated PC of the first leading EOF mode. Compared to the non-  
218 initialised simulation, the models showed no improvement to simulate the first leading EOF  
219 mode of rainfall, but exhibit a better performance in representing the first leading EOF mode  
220 of zonal wind. The CanCM4 and the GFDL-CM2p1 captured the first PC of ua850, but not  
221 the other five models. For the zonal wind at 200 hPa, the BCC-CSM1-1 fails to simulate its  
222 first EOF mode while the other six models can. Only the GFDL-CM2p1 accurately simulates  
223 the first EOF eigenvectors and the associated PC of va850, which cannot be reproduced in the  
224 other models. No models captured the spatial-temporal variation of the first EOF mode of  
225 meridional wind at 200 hPa. In addition, the GFDL-CM2p1 and the MIROC5 simulates a  
226 reasonable leading EOF mode and associated PC of psl, while the other models do not  
227 capture it.

228 Figure 6 shows the fractional (percentage) variances of the six variables from the first  
229 EOF mode with the total variances from the observation, and the model simulation with  
230 (with-out) initialisation. The observational total variances for the pr, the ua850, the ua200, the  
231 va850, the va200 and the psl, are depicted by the first lead EOF mode in 21.2, 59.0, 36.5,  
232 20.6, 28.5 and 50.0 percent, respectively. The models simulated the comparable explanatory  
233 variances, which showed a slight discrepancy for the first leading mode in the non-  
234 initialisation. From non-initialised simulation to initialised simulation, the CGCMs tended to  
235 enhance the first EOF leading mode because they show larger fractional variances of the total



236 variances of the six variables. We note that the CanCM4 and the GFDL-CM2p1 significantly  
237 increased the fractional variances from non-initialisation to initialisation.

238 The ENSO is a dominant mode of the inter-annual variability of the coupled ocean and  
239 atmosphere climate system, which has strong effects on the inter-annual variation of the  
240 EASM (Wang et al., 2000; Wu et al., 2003). Wang et al. (2015) summarised that the first EOF  
241 lead mode of the ASM is ENSO developing mode. As previously mentioned, the first EOF  
242 mode was improved in the initialised simulations, compared to the non-initialised simulation.  
243 This also can be found in the ENSO indices (Figure 7). The individual members and their  
244 ensemble mean of the six models show a low correlation coefficient to the observational  
245 Niño3.4 and the SOI in the non-initialised simulations. These two indices showed strong anti-  
246 phases in the observation, with the correlation range being -0.94 to -0.92 for four seasons  
247 (DJF, MAM, JJA, SON). Without initialisation, the models can describe the anti-correlation  
248 between Niño3.4 and the SOI, but with weaker correlation. Compared to the non-  
249 initialisation, there is a significant improvement for models in capturing the observational  
250 Niño3.4 and the SOI in the initialised experiments. The initialisation lowers the spread of  
251 Niño3.4 and the SOI in all the six models. There is a noticeable change between the model in  
252 producing the relationship between the Niño3.4 and the SOI. We found that the GFDL-  
253 CM2p1 (HadCM3) shows a lower (higher) Niño3.4-SOI correlation in initialisation than that  
254 in non-initialisation. With initialisation, the ensemble mean of each model outperforms its  
255 individual members in capturing Niño3.4 and the SOI, while without initialisation it showed  
256 a worse performance than that of the individual members in simulating Niño3.4 and the SOI.

257 The EASM strongly relies on the pre-seasons ENSO signal due to the lag response of  
258 the atmosphere to the SST anomaly (Wu et al., 2003). The lead-lag correlation coefficients  
259 between the EASM index and the Niño3.4, and the SOI from JJA(-1) to JJA(+1) are  
260 illustrated in Figure 8. The pre-season Niño3.4 (SOI) presents a significant negative  
261 (positive) correlation to the EASM, while the post-season Niño3.4 (SOI) showed a notable  
262 positive (negative) correlation. This lead-lag correlation coefficient phase is called the  
263 Niño3.4-/SOI-EASM coupled mode (Wang et al., 2008b). In the non-initialised cases, the  
264 models do not produce the teleconnection between the ENSO and the EASM. The CanCM4,  
265 the HadCM3 and the MPI-ESM-LR failed to represent the lead-lag correlation coefficient  
266 differences between pre-/post-season ENSO and EASM. The BCC-CSM1-1, the GFDL-  
267 CM2p1 and the MIROC5 captured the coupled mode of the ENSO and the EASM. However,

268 the pre-season ENSO has a weak effect on the EASM. Compared to the non-initialised cases,  
269 the MIROC5 and the GFDL-CM2p1 both demonstrated a significant improvement in  
270 simulating Niño3.4 (SOI)-EASM coupled mode in the initialisation. The BCC-CSM1-1, the  
271 HadCM3, and the HadCM3-ff showed no improvement, with insignificant correlation  
272 between Niño3.4 (SOI) and the EASM. The CanCM4 and the MPI-ESM-LR indicated a  
273 higher correlation between the EASM and the simultaneous-to-post-season ENSO than to the  
274 pre-season ENSO.

## 275 5. DISCUSSION

276 The model exhibits a better performance in simulating the general circulation of the  
277 EASM with initialisation. Thus, initialisation is helpful in forecasting the EASM on a  
278 seasonal time-scale. There are two initialisation methods in our study, full-field initialisation  
279 and anomaly initialisation (Table 1). The full-field initialisation produces more skilful  
280 predictions on the seasonal time-scale in predicting regional temperature and precipitation  
281 (Magnusson et al., 2013;Smith et al., 2013). Nevertheless, for predicting the EASM, there is  
282 no significant difference between the two methods. We can see that both the GFDL-CM2p1  
283 and the MIROC5 have a significant improvement in capturing the EASM, with full-field and  
284 anomaly initialisation, respectively. Only the HadCM3 was initialised by the two  
285 initialisation techniques. However, both these two initialised techniques are producing poor  
286 predictions of the EASM with no major differences.

287 The current initialisation strategy updates the observed atmospheric component (*i.e.*,  
288 zonal and meridional wind, geopotential height, *etc.*) and the SST (Meehl et al., 2009;Taylor  
289 et al., 2012;Meehl et al., 2014). With initialisation, the SST conveys its information via the  
290 large heat content of the ocean to the coupled system. Therefore, an index indicating an ocean  
291 oscillation like Niño3.4 showed a seasonal-to-decadal prediction skill (Jin et al., 2008;Luo et  
292 al., 2008;Choi et al., 2016). The models studied here demonstrated a prediction skill in  
293 simulating Niño3.4 and the SOI due to this effect. The change of the correlation between  
294 Niño3.4 and the SOI is insignificant from non-initialised to initialised simulations. We  
295 therefore conclude that the relationship between Niño3.4 and the SOI depends more on the  
296 model parameterisation than on the initial condition.

297 Wang *et al.* (2015) found that the second EOF mode of ASM is the Indo-western  
298 Pacific monsoon-ocean coupled mode, the third is the Indian Ocean dipole (IOD) mode, and  
299 the fourth is the trend mode. The Indo-western Pacific monsoon-ocean coupled mode is the

300 atmosphere-ocean interaction mode (Wang et al., 2013;Xiang et al., 2013), which is  
301 supported by a positive thermodynamic feedback between the western North Pacific (WNP)  
302 anticyclone and the underlying Indo-Pacific sea surface temperature anomaly dipole over the  
303 warm pool (Wang et al., 2015). The IOD increases the precipitation from the South Asian  
304 subcontinent to southeastern China and suppresses the precipitation over the WNP (Wang et  
305 al., 2015). It affects the Asian monsoon by the meridional asymmetry of the monsoonal  
306 easterly shear during the boreal summer, which can particularly strengthen the northern  
307 branch of the Rossby wave response to the south-eastern Indian Ocean SST cooling, leading  
308 to an intensified monsoon flow as well as an intensified convection (Wang and Xie,  
309 1996;Wang et al., 2003;Xiang et al., 2011;Wang et al., 2015). We noted that the models  
310 simulate a reasonable first EOF mode, but illustrate no skill in capturing the other EOF  
311 leading modes (not shown). We argue that the models cannot well represent the monsoon-  
312 ocean interaction, even with initialisation. The models do not simulate the third EOF leading  
313 mode of the EASM since the predictability of the IOD extends only over a three-month time-  
314 scale (Choudhury et al., 2015). The current initialisation strategies (both anomaly and full  
315 field) enhance the ENSO signal in the model simulations with higher explained fraction of  
316 variance. Kim et al. (2012) described a similar finding in ECMWF System 4 and NCEP  
317 Climate Forecast System version 2 (CFSv2) seasonal prediction simulations. With  
318 initialisation, the models well predict ENSO on seasonal time-scale, which leads to an overly  
319 strong modulation of the EASM by ENSO (Jin et al., 2008;Kim et al., 2012).

320 It is worth mentioning that it was an extremely weak monsoon and strong El Niño year  
321 in 1998. The CanCM4, the GFDL-CM2p1, the MIROC5 and the MPI-ESM-LR have the  
322 ability to simulate the extreme monsoon event, while the BCC-CSM1-1, and the HadCM3 do  
323 not capture it even with initialisation. There is the potential for the BCC-CSM and the  
324 HadCM models to improve the teleconnection between the ENSO and the EASM.

325 This study has discussed six CMIP5 models in predicting the EASM on seasonal time-  
326 scale. The six models are earth system coupled models which present a better SST-monsoon  
327 teleconnection than CMIP3 models (Sperber et al., 2013) and IRI (International Research  
328 Institute for Climate and Society) models (Barnston et al., 2010). There are 4 AGCMs  
329 contributing to the IRI prediction system, including ECHAM4.5, CCM3.6, COLA and  
330 GFDL-AM2p14. These models are forced to forecast the climate on seasonal time-scale by  
331 prescribed SST. Barnston et al. (2010) found that the models showed low prediction skill

332 over East Asia. Therefore, the IRI prediction system cannot be used to predict the EASM.  
333 There are two seasonal forecast application systems, the ECMWF System and the NCEP  
334 CFS, respectively. Both the two application systems have low prediction skill of EASM (Kim  
335 et al., 2012;Jiang et al., 2013). The CMIP5 models have potential to be developed as  
336 application system for EASM seasonal prediction, especially the GFDL-CM2p1 and the  
337 MIROC5.

338 We have compared six CMIP5 systems with their respective initialisation strategies.  
339 The GFDL-CM2p1 and the MIROC5 have the potential to serve as seasonal forecast  
340 application system even with their current initialisation method. These models have great  
341 potential to optimise the SST-EASM interaction simulation performance to improve their  
342 seasonal prediction skill of the EASM.

## 343 **6. SUMMARY**

344 Six earth system models from CMIP5 have been selected in this study. We have analysed the  
345 improvement of the rainfall, the mean sea level pressure, the zonal wind and the meridional  
346 wind in the EASM region from non-initialisation to initialisation. The low prediction skill of  
347 the summer monsoon precipitation is due to the uncertainties of cloud physics and cumulus  
348 parameterisations in the models (Lee et al., 2010;Seo et al., 2015). The models showed a  
349 better performance in capturing the inter-annual variability of zonal wind than the  
350 precipitation after initialisation. Thus, the zonal wind index is an additional factor, which can  
351 indicate the prediction skill of the model. When, we calculate the WF-index in both non-  
352 initialised and initialised simulations, the GFDL-CM2p1 and the MIROC5 showed a  
353 significant advancement in simulating the EASM from non-initialised to initialised  
354 simulation with a lower RMSE and a higher ACC. There is only a slight change in the WF-  
355 index calculated from the BCC-CSM1-1, the CanCM4 and the MPI-ESM-LR data with  
356 initialisation. Compared to the non-initialised simulation, the HadCM3 loses prediction skill,  
357 especially with anomaly initialisation.

358 To test the possible mechanisms of the models' performance in the non-initialisation  
359 and the initialisation, we have calculated the leading mode of the six fields, which are  
360 associated to the EASM. The models demonstrated a better agreement with the observational  
361 first EOF mode in the initialised simulations. The first lead mode of zonal wind at 200 hPa  
362 showed a significant improvement in the models except the BCC-CSM1-1 with initialisation.  
363 Therefore, a potential predictor might be an index based upon the zonal wind at 200 hPa.

364 Compared to the non-initialisation, the models enhanced the first EOF mode with a higher  
365 fraction of variance to the total variance after initialisation. The first EOF mode of the EASM  
366 is the ENSO developing mode (Wang et al., 2015). We have analysed the seasonal simulating  
367 skill of Niño3.4 and the SOI in each model. The models showed a poor performance in  
368 representing Niño3.4 and the SOI in the non-initialised simulation. Initialisation improved the  
369 model simulating skill of Niño3.4 and the SOI. The initialised simulations decreased the  
370 spread of ensemble members in the models. We found that there is no significant change in  
371 the models reproducing the correlation between Niño3.4 and the SOI from non-initialisation  
372 to initialisation.

373 In general, the pre-season warm phase of the ENSO (El Niño) leads to a weak EASM  
374 producing more rainfall over the South China Sea and northwest China, and less rainfall over  
375 the Yangtze River Valley and the southern Japan; the cold phase of the ENSO (La Niña)  
376 illustrated a reverse rainfall pattern to El Niño in East Asia. The pre-season Niño3.4 (SOI)  
377 exhibits a strong negative (positive) correlation to the EASM, while the correlation between  
378 the post-season Niño3.4 (SOI) and the EASM illustrated an anti-phase as the pre-season. In  
379 the non-initialised simulations, the models do not capture Niño3.4-/SOI-EASM coupled  
380 mode. We found that only the MIROC5 has the ability to represent the Niño3.4-EASM  
381 coupled mode with initialisation. For the SOI-EASM coupled mode, the GFDL-CM2p1 and  
382 the MIROC5 captured it in the initialisation, while the BCC-CSM1-1, the HadCM3, the  
383 HadCM2-ff, the CanCM4 and the MPI-ESM-LR do not. Therefore, we argue that the  
384 differential depiction of ENSO-EASM coupled mode in CMIP5 models lead to their  
385 differential response to initialisation.

### 386 **Acknowledgements**

387 The China Scholarship Council (CSC) and the Freie Universität Berlin supported this work.  
388 We would like to thank the climate modelling groups listed in Table 1 of this paper for  
389 producing and making their model output available. We acknowledge the MiKlip project  
390 funded by the Federal Ministry of Education and Research and the German Climate  
391 Computing Centre (DKRZ) for providing the data services. We are grateful to Mrs  
392 Margerison Patricia for her useful comments and the proofreading work on this manuscript.

### 393 **References**

394 Adler, R. F., Huffman, G. J., Chang, A., Ferraro, R., Xie, P.-P., Janowiak, J., Rudolf, B.,  
395 Schneider, U., Curtis, S., Bolvin, D., Gruber, A., Susskind, J., Arkin, P., and Nelkin, E.: The  
396 Version-2 Global Precipitation Climatology Project (GPCP) Monthly Precipitation Analysis

397 (1979–Present), *J Hydrometeorol*, 4, 1147-1167, 10.1175/1525-  
398 7541(2003)004<1147:tvGPCP>2.0.CO;2, 2003.

399 Arora, V. K., Scinocca, J. F., Boer, G. J., Christian, J. R., Denman, K. L., Flato, G. M.,  
400 Kharin, V. V., Lee, W. G., and Merryfield, W. J.: Carbon emission limits required to satisfy  
401 future representative concentration pathways of greenhouse gases, *Geophys Res Lett*, 38,  
402 L05805, 10.1029/2010gl046270, 2011.

403 Barnett, T. P., and Schlesinger, M. E.: Detecting Changes in Global Climate Induced by  
404 Greenhouse Gases, *J Geophys Res Atmos*, 92, 14772-14780, 10.1029/JD092iD12p14772,  
405 1987.

406 Barnston, A. G., Li, S. H., Mason, S. J., DeWitt, D. G., Goddard, L., and Gong, X. F.:  
407 Verification of the First 11 Years of IRI's Seasonal Climate Forecasts, *J Appl Meteorol Clim*,  
408 49, 493-520, 10.1175/2009jamc2325.1, 2010.

409 Choi, J., Son, S. W., Ham, Y. G., Lee, J. Y., and Kim, H. M.: Seasonal-to-Interannual  
410 Prediction Skills of Near-Surface Air Temperature in the CMIP5 Decadal Hindcast  
411 Experiments, *J Clim*, 29, 1511-1527, 10.1175/Jcli-D-15-0182.1, 2016.

412 Choudhury, D., Sharma, A., Sivakumar, B., Sen Gupta, A., and Mehrotra, R.: On the  
413 predictability of SSTA indices from CMIP5 decadal experiments, *Environ Res Lett*, 10,  
414 074013, 10.1088/1748-9326/10/7/074013, 2015.

415 Dee, D. P., Uppala, S. M., Simmons, A. J., Berrisford, P., Poli, P., Kobayashi, S., Andrae, U.,  
416 Balmaseda, M. A., Balsamo, G., Bauer, P., Bechtold, P., Beljaars, A. C. M., van de Berg, L.,  
417 Bidlot, J., Bormann, N., Delsol, C., Dragani, R., Fuentes, M., Geer, A. J., Haimberger, L.,  
418 Healy, S. B., Hersbach, H., Holm, E. V., Isaksen, I., Kallberg, P., Kohler, M., Matricardi, M.,  
419 McNally, A. P., Monge-Sanz, B. M., Morcrette, J. J., Park, B. K., Peubey, C., de Rosnay, P.,  
420 Tavolato, C., Thepaut, J. N., and Vitart, F.: The ERA-Interim reanalysis: configuration and  
421 performance of the data assimilation system, *Q J R Meteorol Soc*, 137, 553-597,  
422 10.1002/qj.828, 2011.

423 Delworth, T. L., Broccoli, A. J., Rosati, A., Stouffer, R. J., Balaji, V., Beesley, J. A., Cooke,  
424 W. F., Dixon, K. W., Dunne, J., Dunne, K. A., Durachta, J. W., Findell, K. L., Ginoux, P.,  
425 Gnanadesikan, A., Gordon, C. T., Griffies, S. M., Gudgel, R., Harrison, M. J., Held, I. M.,  
426 Hemler, R. S., Horowitz, L. W., Klein, S. A., Knutson, T. R., Kushner, P. J., Langenhorst, A.  
427 R., Lee, H. C., Lin, S. J., Lu, J., Malyshev, S. L., Milly, P. C. D., Ramaswamy, V., Russell, J.,  
428 Schwarzkopf, M. D., Shevliakova, E., Sirutis, J. J., Spelman, M. J., Stern, W. F., Winton, M.,  
429 Wittenberg, A. T., Wyman, B., Zeng, F., and Zhang, R.: GFDL's CM2 global coupled climate  
430 models. Part I: Formulation and simulation characteristics, *J Clim*, 19, 643-674,  
431 10.1175/Jcli3629.1, 2006.

432 Ding, Y.: Seasonal march of the East-Asian summer monsoon., in: *East Asian Monsoon*,  
433 edited by: Chang, C.-P., World Scientific, Singapore, 560, 2004.

434 Ding, Y. H.: *Monsoons over China*, Kluwer Academic Publisher, Dordrecht/Boston/London,  
435 419 pp., 1994.

436 Ding, Y. H., and Chan, J. C. L.: The East Asian summer monsoon: an overview, *Meteorol*  
437 *Atmos Phys*, 89, 117-142, 10.1007/s00703-005-0125-z, 2005.

438 Drosowsky, W., and Zhang, H.: Verification of Spatial Fields, in: *Forecast Verification: A*  
439 *Practitioner's Guide in Atmospheric Science* edited by: Jolliffe, L. T., and Stephenson, D. B.,  
440 John Wiley & Sons Ltd, England, 128-129, 2003.

441 Goddard, L., Mason, S. J., Zebiak, S. E., Ropelewski, C. F., Basher, R., and Cane, M. A.:  
442 Current approaches to seasonal-to-interannual climate predictions, *Int J Climatol*, 21, 1111-  
443 1152, 10.1002/joc.636, 2001.

444 Huang, B. Y., Banzon, V. F., Freeman, E., Lawrimore, J., Liu, W., Peterson, T. C., Smith, T.  
445 M., Thorne, P. W., Woodruff, S. D., and Zhang, H. M.: Extended Reconstructed Sea Surface

446 Temperature Version 4 (ERSST.v4). Part I: Upgrades and Intercomparisons, *J Clim*, 28, 911-  
447 930, 10.1175/Jcli-D-14-00006.1, 2015.

448 Jiang, X. W., Yang, S., Li, Y. Q., Kumar, A., Liu, X. W., Zuo, Z. Y., and Jha, B.: Seasonal-  
449 to-Interannual Prediction of the Asian Summer Monsoon in the NCEP Climate Forecast  
450 System Version 2, *J Clim*, 26, 3708-3727, 10.1175/Jcli-D-12-00437.1, 2013.

451 Jin, E. K., Kinter, J. L., Wang, B., Park, C. K., Kang, I. S., Kirtman, B. P., Kug, J. S., Kumar,  
452 A., Luo, J. J., Schemm, J., Shukla, J., and Yamagata, T.: Current status of ENSO prediction  
453 skill in coupled ocean-atmosphere models, *Clim Dyn*, 31, 647-664, 10.1007/s00382-008-  
454 0397-3, 2008.

455 Kang, I.-S., and Shukla, J.: Dynamic seasonal prediction and predictability of the monsoon,  
456 in: *The Asian Monsoon*, edited by: Wang, B., Springer Berlin Heidelberg, Berlin, Heidelberg,  
457 585-612, 2006.

458 Kang, I. S., and Yoo, J. H.: Examination of multi-model ensemble seasonal prediction  
459 methods using a simple climate system, *Clim Dyn*, 26, 285-294, 10.1007/s00382-005-0074-8,  
460 2006.

461 Kim, H. J., Wang, B., and Ding, Q. H.: The Global Monsoon Variability Simulated by  
462 CMIP3 Coupled Climate Models, *J Clim*, 21, 5271-5294, 10.1175/2008jcli2041.1, 2008.

463 Kim, H. J., Takata, K., Wang, B., Watanabe, M., Kimoto, M., Yokohata, T., and Yasunari, T.:  
464 Global Monsoon, El Nino, and Their Interannual Linkage Simulated by MIROC5 and the  
465 CMIP3 CGCMs, *J Clim*, 24, 5604-5618, 10.1175/2011jcli4132.1, 2011.

466 Kim, H. M., Webster, P. J., Curry, J. A., and Toma, V. E.: Asian summer monsoon prediction  
467 in ECMWF System 4 and NCEP CFSv2 retrospective seasonal forecasts, *Clim Dyn*, 39,  
468 2975-2991, 10.1007/s00382-012-1470-5, 2012.

469 Kug, J. S., Kang, I. S., and Choi, D. H.: Seasonal climate predictability with Tier-one and  
470 Tier-two prediction systems, *Clim Dyn*, 31, 403-416, DOI 10.1007/s00382-007-0264-7, 2008.

471 Lee, J.-Y., Wang, B., Kang, I. S., Shukla, J., Kumar, A., Kug, J. S., Schemm, J. K. E., Luo, J.  
472 J., Yamagata, T., Fu, X., Alves, O., Stern, B., Rosati, T., and Park, C. K.: How are seasonal  
473 prediction skills related to models' performance on mean state and annual cycle?, *Clim Dyn*,  
474 35, 267-283, 10.1007/s00382-010-0857-4, 2010.

475 Luo, J.-J., Masson, S., Behera, S. K., and Yamagata, T.: Extended ENSO Predictions Using a  
476 Fully Coupled Ocean-Atmosphere Model, *J Clim*, 21, 84-93, 10.1175/2007jcli1412.1, 2008.

477 Magnusson, L., Alonso-Balmaseda, M., Corti, S., Molteni, F., and Stockdale, T.: Evaluation  
478 of forecast strategies for seasonal and decadal forecasts in presence of systematic model  
479 errors, *Clim Dyn*, 41, 2393-2409, 10.1007/s00382-012-1599-2, 2013.

480 Matei, D., Pohlmann, H., Jungclaus, J., Muller, W., Haak, H., and Marotzke, J.: Two Tales of  
481 Initializing Decadal Climate Prediction Experiments with the ECHAM5/MPI-OM Model, *J*  
482 *Clim*, 25, 8502-8523, 10.1175/Jcli-D-11-00633.1, 2012.

483 Meehl, G., Covey, C., Delworth, T., Latif, M., McAvaney, B., Mitchell, J., Stouffer, R., and  
484 Taylor, K.: The WCRP CMIP3 multi-model dataset: a new era in climate change research,  
485 *Bull Am Meteorol Soc*, 88, 1383-1394, 2007.

486 Meehl, G. A., Goddard, L., Murphy, J., Stouffer, R. J., Boer, G., Danabasoglu, G., Dixon, K.,  
487 Giorgetta, M. A., Greene, A. M., Hawkins, E., Hegerl, G., Karoly, D., Keenlyside, N.,  
488 Kimoto, M., Kirtman, B., Navarra, A., Pulwarty, R., Smith, D., Stammer, D., and Stockdale,  
489 T.: DECADAL PREDICTION Can It Be Skillful?, *Bull Am Meteorol Soc*, 90, 1467-1485,  
490 10.1175/2009bams2778.1, 2009.

491 Meehl, G. A., and Teng, H. Y.: Case studies for initialized decadal hindcasts and predictions  
492 for the Pacific region, *Geophys Res Lett*, 39, L22705, 10.1029/2012gl053423, 2012.

493 Meehl, G. A., Goddard, L., Boer, G., Burgman, R., Branstator, G., Cassou, C., Corti, S.,  
494 Danabasoglu, G., Doblas-Reyes, F., Hawkins, E., Karspeck, A., Kimoto, M., Kumar, A.,

495 Matei, D., Mignot, J., Msadek, R., Navarra, A., Pohlmann, H., Rienecker, M., Rosati, T.,  
496 Schneider, E., Smith, D., Sutton, R., Teng, H. Y., van Oldenborgh, G. J., Vecchi, G., and  
497 Yeager, S.: DECADAL CLIMATE PREDICTION An Update from the Trenches, *Bull Am*  
498 *Meteorol Soc*, 95, 243-267, 10.1175/Bams-D-12-00241.1, 2014.

499 Mitchell, J. F. B., Karoly, D. J., Hegerl, G. C., Zwiers, F. W., Allen, M. R., and Marengo, J.:  
500 Detection of Climate Change and Attribution of Causes, in: *Third Assessment Report of the*  
501 *Intergovernmental Panel on Climate Change.*, edited by: Houghton, J. T., Griggs, D. J.,  
502 Noguer, M., van der Linden, P. J., Dai, X., Maskell, K., and Johnson, C. A., Cambridge  
503 University Press, New York, 470, 2001.

504 Seo, K. H., Son, J. H., Lee, J. Y., and Park, H. S.: Northern East Asian Monsoon Precipitation  
505 Revealed by Airmass Variability and Its Prediction, *J Clim*, 28, 6221-6233, 10.1175/Jcli-D-  
506 14-00526.1, 2015.

507 Smith, D. M., Eade, R., and Pohlmann, H.: A comparison of full-field and anomaly  
508 initialization for seasonal to decadal climate prediction, *Clim Dyn*, 41, 3325-3338,  
509 10.1007/s00382-013-1683-2, 2013.

510 Sperber, K., Annamalai, H., Kang, I. S., Kitoh, A., Moise, A., Turner, A., Wang, B., and  
511 Zhou, T.: The Asian summer monsoon: an intercomparison of CMIP5 vs. CMIP3 simulations  
512 of the late 20th century, *Clim Dyn*, 41, 2711-2744, 10.1007/s00382-012-1607-6, 2013.

513 Sperber, K. R., Brankovic, C., Deque, M., Frederiksen, C. S., Graham, R., Kitoh, A.,  
514 Kobayashi, C., Palmer, T., Puri, K., Tennant, W., and Volodin, E.: Dynamical seasonal  
515 predictability of the Asian summer monsoon, *Mon Weather Rev*, 129, 2226-2248,  
516 10.1175/1520-0493(2001)129<2226:Dspota>2.0.Co;2, 2001.

517 Tao, S. Y., and Chen, L. X.: A review of recent research on the East Asian summer monsoon  
518 in China, in: *Monsoon Meteorology*, edited by: Chang, C.-P., and Krishnamurti, T. N., Oxford  
519 University Press, Oxford, 60-92, 1987.

520 Tatebe, H., Ishii, M., Mochizuki, T., Chikamoto, Y., Sakamoto, T. T., Komuro, Y., Mori, M.,  
521 Yasunaka, S., Watanabe, M., Ogochi, K., Suzuki, T., Nishimura, T., and Kimoto, M.: The  
522 Initialization of the MIROC Climate Models with Hydrographic Data Assimilation for  
523 Decadal Prediction, *J Meteorol Soc Japan*, 90a, 275-294, 10.2151/jmsj.2012-A14, 2012.

524 Taylor, K. E., Stouffer, R. J., and Meehl, G. A.: An Overview of CMIP5 and the Experiment  
525 Design, *Bull Am Meteorol Soc*, 93, 485-498, 10.1175/Bams-D-11-00094.1, 2012.

526 Wang, B., and Xie, X.: Low-Frequency Equatorial Waves in Vertically Sheared Zonal Flow.  
527 Part I: Stable Waves, *J Atmos Sci*, 53, 449-467, 10.1175/1520-  
528 0469(1996)053<0449:lfewiv>2.0.co;2, 1996.

529 Wang, B., and Fan, Z.: Choice of south Asian summer monsoon indices, *Bull Am Meteorol*  
530 *Soc*, 80, 629-638, 10.1175/1520-0477(1999)080<0629:Cosasm>2.0.Co;2, 1999.

531 Wang, B., Wu, R. G., and Fu, X. H.: Pacific-East Asian teleconnection: how does ENSO  
532 affect East Asian climate?, *J Clim*, 13, 1517-1536, 2000.

533 Wang, B., Wu, R., and Li, T.: Atmosphere–Warm Ocean Interaction and Its Impacts on  
534 Asian–Australian Monsoon Variation\*, *J Clim*, 16, 1195-1211, 10.1175/1520-  
535 0442(2003)16<1195:aoiaii>2.0.co;2, 2003.

536 Wang, B., Kang, I.-S., and Lee, J.-Y.: Ensemble Simulations of Asian–Australian Monsoon  
537 Variability by 11 AGCMs\*, *J Clim*, 17, 803-818, 10.1175/1520-  
538 0442(2004)017<0803:esoamv>2.0.co;2, 2004.

539 Wang, B., Ding, Q. H., Fu, X. H., Kang, I. S., Jin, K., Shukla, J., and Doblus-Reyes, F.:  
540 Fundamental challenge in simulation and prediction of summer monsoon rainfall, *Geophys*  
541 *Res Lett*, 32, L15711, 10.1029/2005gl022734, 2005.

542 Wang, B.: *The Asian Monsoon*, Springer Science & Business Media, Praxis, New York, NY,  
543 USA, 2006.



544 Wang, B., Lee, J.-Y., Kang, I.-S., Shukla, J., Park, C. K., Kumar, A., Schemm, J., Cocke, S.,  
 545 Kug, J. S., Luo, J. J., Zhou, T., Wang, B., Fu, X., Yun, W. T., Alves, O., Jin, E. K., Kinter, J.,  
 546 Kirtman, B., Krishnamurti, T., Lau, N. C., Lau, W., Liu, P., Pegion, P., Rosati, T., Schubert,  
 547 S., Stern, W., Suarez, M., and Yamagata, T.: Advance and prospectus of seasonal prediction:  
 548 assessment of the APCC/CLIPAS 14-model ensemble retrospective seasonal prediction  
 549 (1980–2004), *Clim Dyn*, 33, 93-117, 10.1007/s00382-008-0460-0, 2008a.  
 550 Wang, B., Wu, Z. W., Li, J. P., Liu, J., Chang, C. P., Ding, Y. H., and Wu, G. X.: How to  
 551 measure the strength of the East Asian summer monsoon, *J Clim*, 21, 4449-4463,  
 552 10.1175/2008jcli2183.1, 2008b.  
 553 Wang, B., Xiang, B., and Lee, J. Y.: Subtropical high predictability establishes a promising  
 554 way for monsoon and tropical storm predictions, *Proc Natl Acad Sci U S A*, 110, 2718-2722,  
 555 10.1073/pnas.1214626110, 2013.  
 556 Wang, B., Lee, J. Y., and Xiang, B. Q.: Asian summer monsoon rainfall predictability: a  
 557 predictable mode analysis, *Clim Dyn*, 44, 61-74, 10.1007/s00382-014-2218-1, 2015.  
 558 Wu, R. G., Hu, Z. Z., and Kirtman, B. P.: Evolution of ENSO-related rainfall anomalies in  
 559 East Asia, *J Clim*, 16, 3742-3758, 10.1175/1520-0442(2003)016<3742:Eoerai>2.0.Co;2,  
 560 2003.  
 561 Wu, T. W., Song, L. C., Li, W. P., Wang, Z. Z., Zhang, H., Xin, X. G., Zhang, Y. W., Zhang,  
 562 L., Li, J. L., Wu, F. H., Liu, Y. M., Zhang, F., Shi, X. L., Chu, M., Zhang, J., Fang, Y. J.,  
 563 Wang, F., Lu, Y. X., Liu, X. W., Wei, M., Liu, Q. X., Zhou, W. Y., Dong, M., Zhao, Q. G., Ji,  
 564 J. J., Li, L., and Zhou, M. Y.: An Overview of BCC Climate System Model Development and  
 565 Application for Climate Change Studies, *J Meteorol Res-Prc*, 28, 34-56, 10.1007/s13351-  
 566 014-3041-7, 2014.  
 567 Wu, Z. W., Wang, B., Li, J. P., and Jin, F. F.: An empirical seasonal prediction model of the  
 568 east Asian summer monsoon using ENSO and NAO, *J Geophys Res Atmos*, 114, D18120,  
 569 10.1029/2009jd011733, 2009.  
 570 Xiang, B., Wang, B., Yu, W., and Xu, S.: How can anomalous western North Pacific  
 571 Subtropical High intensify in late summer?, *Geophys Res Lett*, 40, 2349-2354,  
 572 10.1002/grl.50431, 2013.  
 573 Xiang, B. Q., Yu, W. D., Li, T., and Wang, B.: The critical role of the boreal summer mean  
 574 state in the development of the IOD, *Geophys Res Lett*, 38, L02710, 10.1029/2010gl045851,  
 575 2011.  
 576 Yang, S., Zhang, Z. Q., Kousky, V. E., Higgins, R. W., Yoo, S. H., Liang, J. Y., and Fan, Y.:  
 577 Simulations and seasonal prediction of the Asian summer monsoon in the NCEP Climate  
 578 Forecast System, *J Clim*, 21, 3755-3775, 10.1175/2008jcli1961.1, 2008.  
 579 Yim, S. Y., Wang, B., and Xing, W.: Prediction of early summer rainfall over South China by  
 580 a physical-empirical model, *Clim Dyn*, 43, 1883-1891, 10.1007/s00382-013-2014-3, 2014.  
 581 Zhou, T., Wu, B., and Wang, B.: How Well Do Atmospheric General Circulation Models  
 582 Capture the Leading Modes of the Interannual Variability of the Asian–Australian Monsoon?,  
 583 *J Clim*, 22, 1159-1173, 10.1175/2008jcli2245.1, 2009.  
 584 Zhou, T. J., and Yu, R. C.: Atmospheric water vapor transport associated with typical  
 585 anomalous summer rainfall patterns in China, *J Geophys Res Atmos*, 110, D08104,  
 586 10.1029/2004jd005413, 2005.  
 587

Table 1. Details of the prediction systems investigated in this study.

System	Institute	Resolution		Non- Initialisation		Initialisation Type	Reference
		Atmospheric	Oceanic	Members	Members		
BCC-CSM1-1	Beijing Climate Center, China	T42L26	1lonx1.33lat L40	3	3	Full-field	Wu <i>et al.</i> (2014)
CanCM4	Canadian Centre for Climate Modelling and Analysis, Canada	T63L35	256 x 192 L40	10	10	Full-field	Arora <i>et al.</i> (2011)
GFDL-CM2p1	Geophysical Fluid Dynamics Laboratory, USA	N45L24	1lon x 0.33-1lat L50	10	10	Full-field	Delworth <i>et al.</i> (2006)
HadCM3	Met Office Hadley Centre, UK	N48L19	1.25x1.25 L20	10	10 + 10	Full-field and Anomaly	Smith <i>et al.</i> (2013)
MIROC5	Atmosphere and Ocean Research Institute, Japan	T85L40	256x192 L44	5	6	Anomaly	Tatebe <i>et al.</i> (2012)
MPI-ESM-LR	Max Planck Institute for Meteorology, Germany	T63L47	GR15 L40	3	3	Anomaly	Matei <i>et al.</i> (2012)

590 Table 2. Brief summaries of initialisation strategies used by modelling groups in the study. ECMWF: European Centre for Medium-Range  
 591 Weather Forecasts; GODAS: Global Ocean Data Assimilation System; NCEP: National Centers for Environmental Prediction; S: Salinity;  
 592 SODA: Simple Ocean Data Assimilation; T: Temperature.

system	Atmosphere	Ocean	Initialised date	Internet
BCC-CSM1-1	-	integration with ocean T nudged to SODA product above 1500 m	Ensemble 1: 1 <sup>st</sup> September Ensemble 2: 1 <sup>st</sup> November Ensemble 3: 1 <sup>st</sup> January	<a href="http://forecast.bccsm.ncc-cma.net/">http://forecast.bccsm.ncc-cma.net/</a>
CanCM4	ECMWF re-analysis	off-line assimilation of SODA and GODAS subsurface ocean T and S adjusted to reserve model T-S	1 <sup>st</sup> January	<a href="http://www.cccma.ec.gc.ca/">http://www.cccma.ec.gc.ca/</a>
GFDL-CM2p1	GFDL re-analysis	assimilates observations of T, S from World Ocean Database	1 <sup>st</sup> November	<a href="https://www.gfdl.noaa.gov/multidecadal-prediction-stream/">https://www.gfdl.noaa.gov/multidecadal-prediction-stream/</a>
HadCM3	ECMWF re-analysis	off-line ocean re-analysis product	1 <sup>st</sup> January	<a href="http://cerawww.dkrz.de/WDCC/CMIP5/">http://cerawww.dkrz.de/WDCC/CMIP5/</a>
MIROC5	-	integration using observational gridded ocean T and S	1 <sup>st</sup> January	<a href="http://amaterasu.ees.hokudai.ac.jp/">http://amaterasu.ees.hokudai.ac.jp/</a>
MPI-ESM-LR	NCEP re-analysis	off-line ocean hindcast forced with NCEP	1 <sup>st</sup> January	<a href="http://cerawww.dkrz.de/WDCC/CMIP5/">http://cerawww.dkrz.de/WDCC/CMIP5/</a>

593

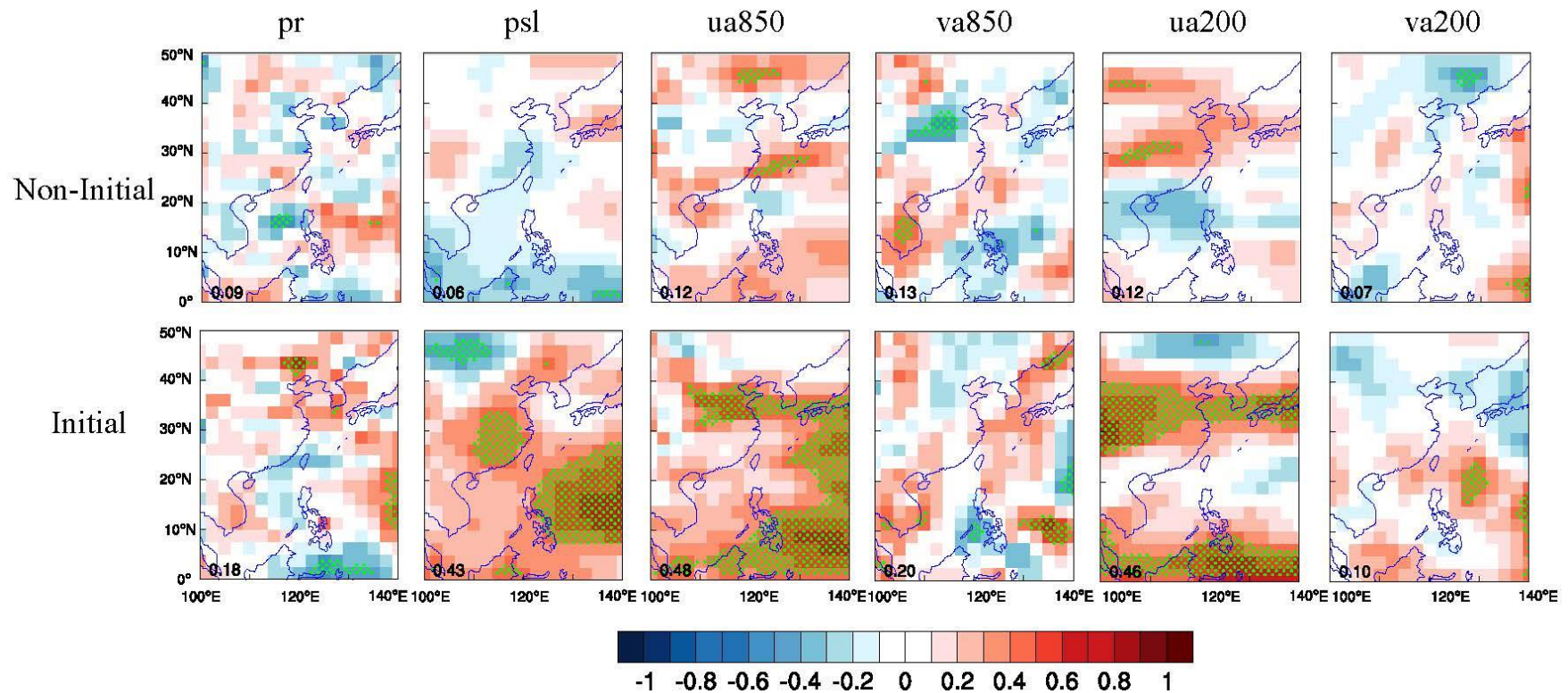
594 Table 3. Description of the six variables which contribute to the EASM. The abbreviation of these variables is followed to the guidelines of  
 595 CMIP5.

variable	Standard name	Contribution to the EASM
pr	Precipitation	Precipitation distribution indicates the strength of EASM
psl	Mean sea surface pressure	Differences of mean sea surface pressure between land and ocean lead to EASM
ua850	Zonal winds over 850 hPa	A component of low-level cyclone which transports vapor from ocean to land
va850	Meridional winds over 850 hPa	As ua850, and contributes to Hadley's cell
va200	Meridional winds over 850 hPa	A component of upper-level Hadley's cell
ua200	Zonal winds over 850 hPa	As va200

596

597

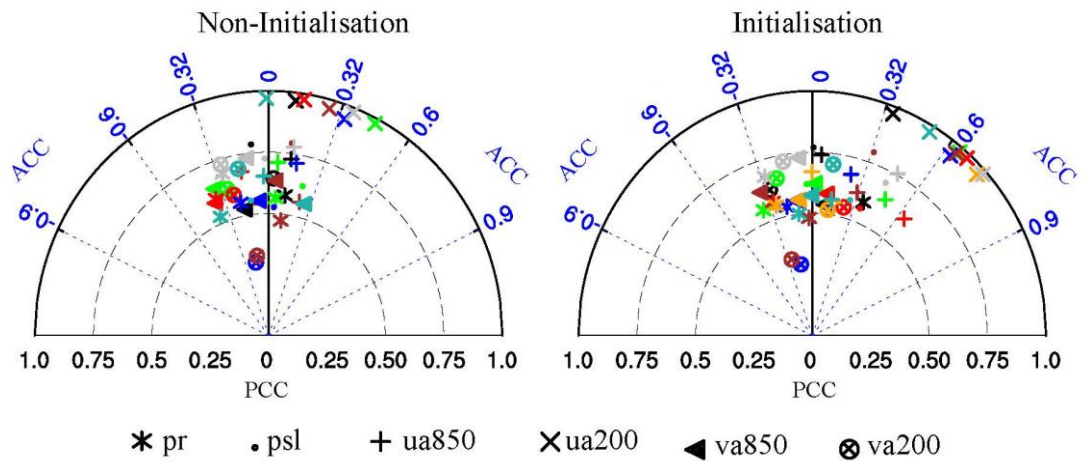
598



599

600 Fig. 1. Anomaly correlation coefficient of six variables (i.e. precipitation, mean sea level pressure, and winds over 850 hPa and 200 hPa)  
 601 between multi-model ensemble mean and observations in non-initialisation and initialisation. The green dotted grids illustrate the significant  
 602 level at 0.05. The number at lower left corner indicates the ratio of significant grid points to entire grids. The GPCP was employed as the  
 603 reference data for precipitation (pr) while winds (i.e. ua850, va850, ua200 and va200) and mean sea level pressure (psl) were compared with  
 604 ERA-Interim re-analysis.

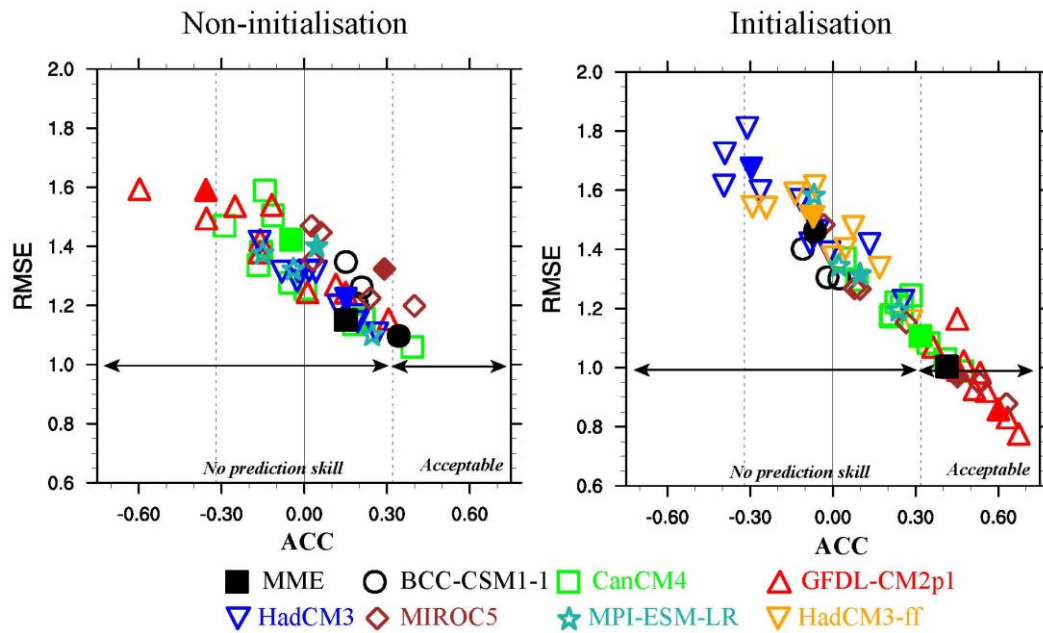
605



606

607 Fig.2. Taylor diagrams display of pattern (PCC) and temporal (ACC) correlation  
608 metrics of six variables between observation and model simulation in the EASM  
609 region (0-50°N, 100-140°E). Each coloured marker represents a model, *i.e.*, the BCC-  
610 CSM1-1 (black), the CanCM4 (green), the GFDL-CM2p1 (red), the HadCM3 (blue),  
611 the MIROC5 (brown), the MPI-ESM-LR (light-sea-blue), and the HadCM3-ff  
612 (orange).

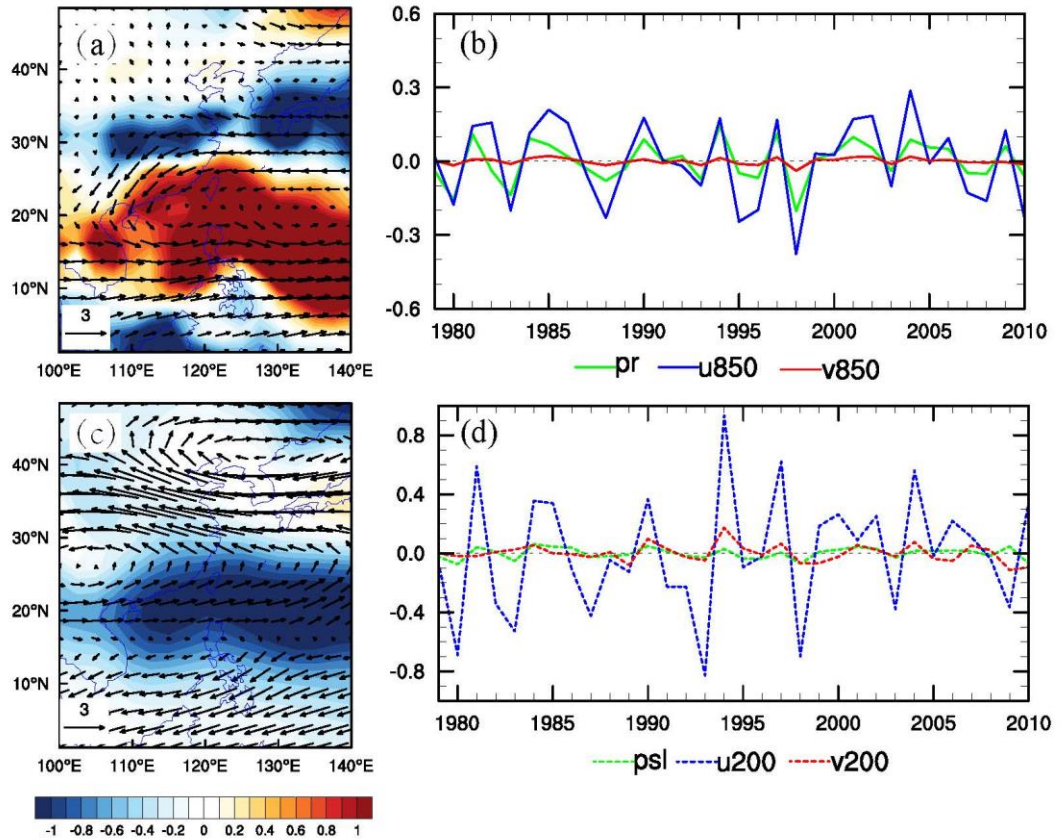
613



615

616 Fig. 3. Performance of the model ensemble member (hollow marker) and its ensemble  
 617 mean (solid marker) on the EASM index. The abscissa and ordinates are the anomaly  
 618 correlation coefficient (ACC) and the root-mean-square-error (RMSE), respectively.  
 619 The observed EASM index is calculated by zonal wind at 850 hPa from the ERA-  
 620 Interim re-analysis data. The black dot lines indicate the significant level at 0.1. The  
 621 vertical black line represents the correlation between the simulating and the  
 622 observational EASM index is 0.





623

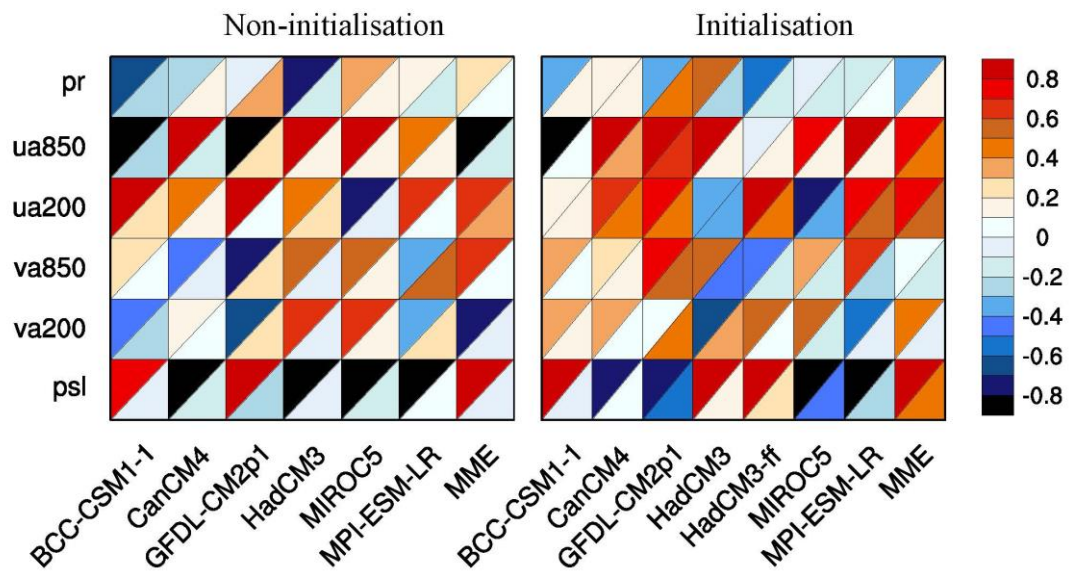
624 Fig. 4. Spatial distribution of observational of the first leading EOF mode of June-  
 625 July-August precipitation and winds over 850 hPa (a), mean sea level pressure and  
 626 winds over 200 hPa (c) and the associated principal component (PC; b, d). The GPCP  
 627 and ERA-Interim data from 1979-2005 were used for the EOF analysis in the EASM  
 628 domain.

629



630

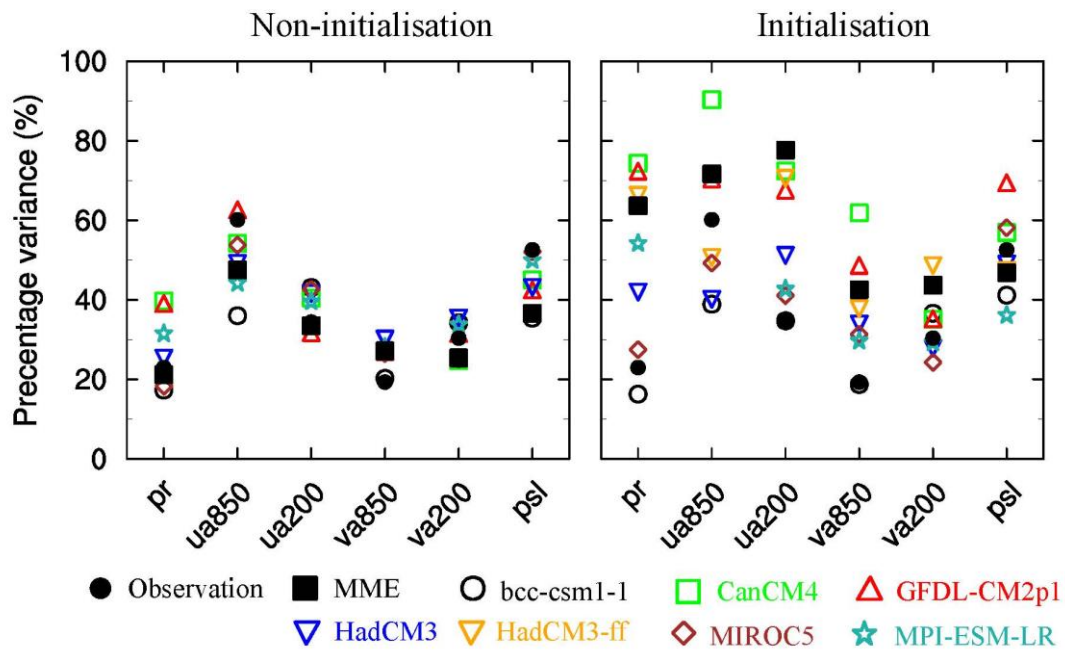
631



632

633 Fig. 5. Portrait diagram display of correlation metrics between the observation and the  
634 model simulation of the first lead EOF mode for the six fields in the non-initialisation  
635 (left) and the initialisation (right). Each grid square is split by a diagonal in order to  
636 show the correlation with respect to both the eigenvector (upper left triangle) and its  
637 associated principal components (lower right triangle) reference data sets.

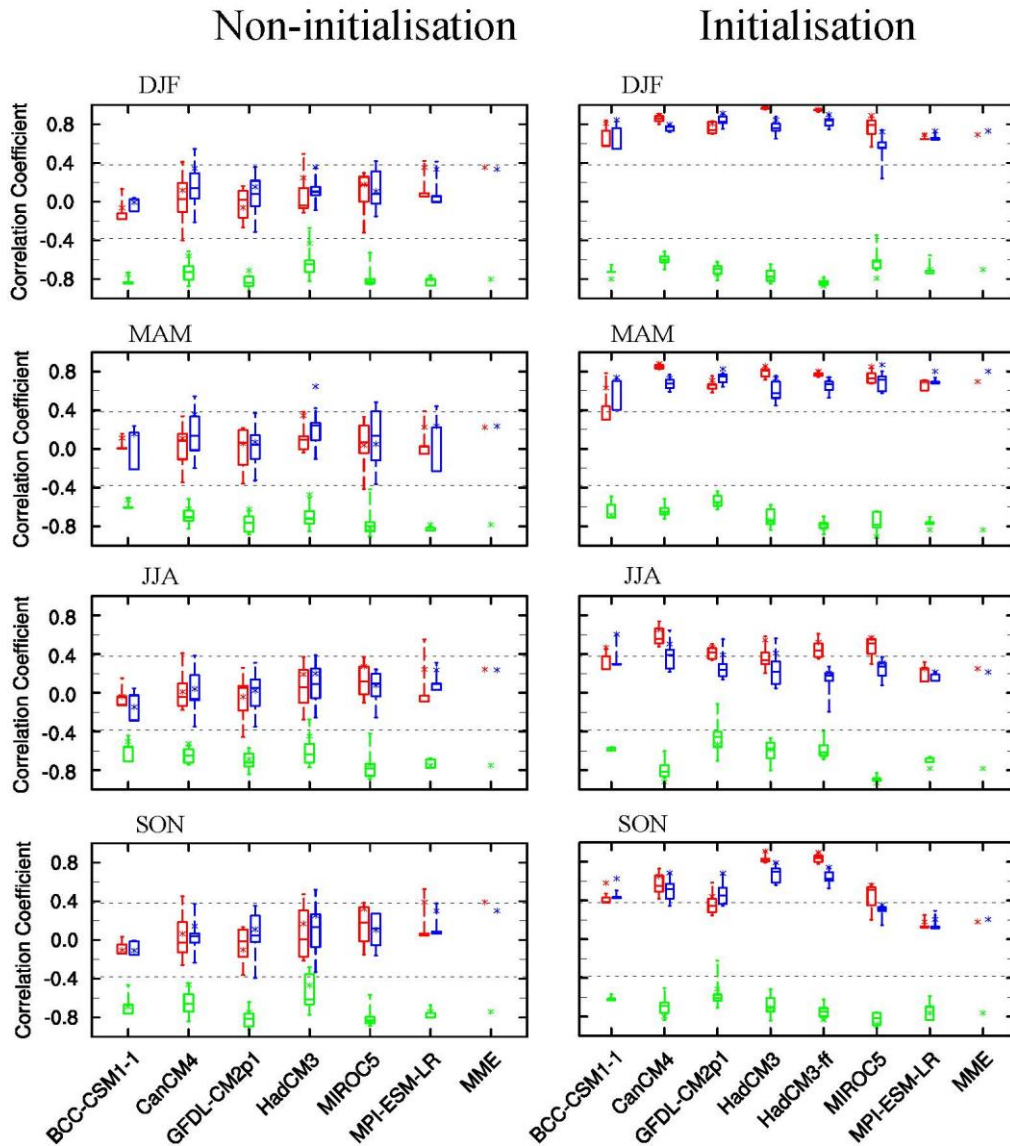
638



640

641 Fig. 6. Fraction variance (%) explained by the first EOF mode for six fields in the  
 642 non-initialisation (left) and the initialisation (right).

643



644

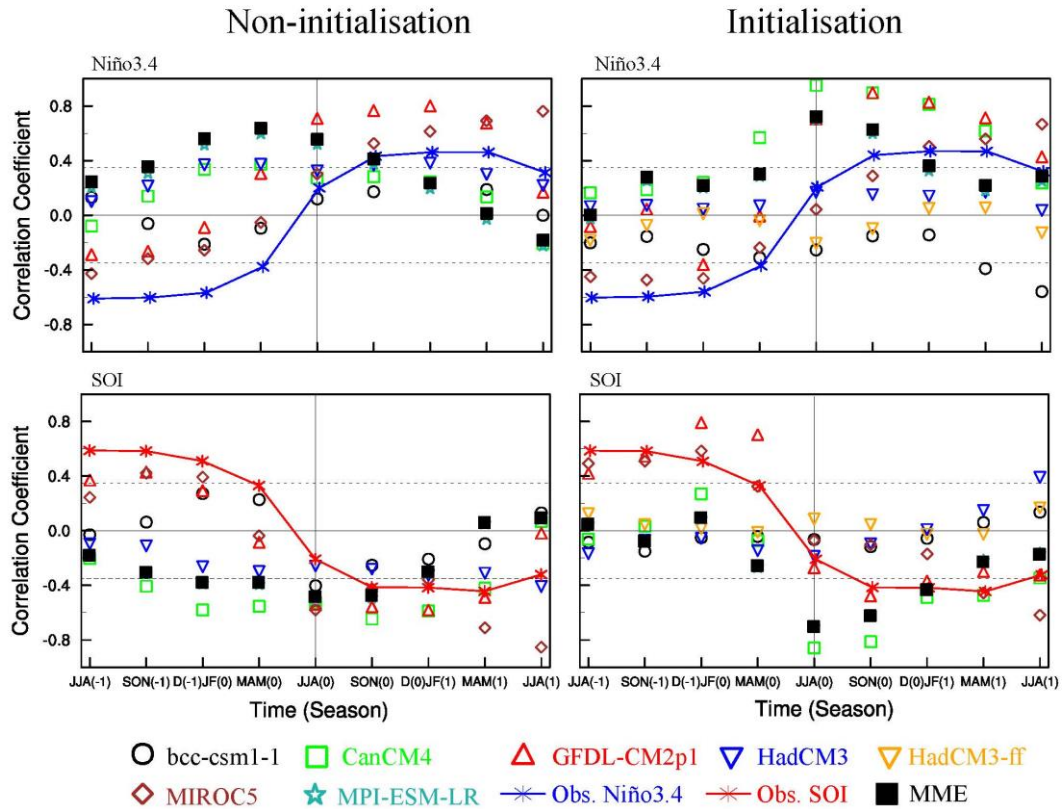
645 Fig. 7. Model prediction skill in representing the observational Niño3.4 (red), the SOI  
 646 (blue) from the DJF to SON in non-initialisation (left) and initialisation (right). Green  
 647 diagram shows the correlation coefficient between the model simulated Niño3.4 and  
 648 the SOI. Box and whisker diagram shows ensemble mean of each model (asterisk),  
 649 median (horizontal line), 25th and 75th percentiles (box), minimum and maximum  
 650 (whisker). The two black dotted lines indicate 0.05 significant level based upon  
 651 Student's t-test.

652

653

654

655



656

657 Fig. 8. Lead-lag correlation coefficients between the EASM index and Niño3.4  
 658 (upper), and SOI (lower) in non-initialised simulations (left) and initialised ones  
 659 (right) for observation (marker line) and models (marker) from JJA(-1) to JJA(+1).  
 660 The two black dotted lines are 0.05 significant level based upon Student's t-test. The  
 661 vertical line represents JJA(0), where the simultaneous correlations between the  
 662 EASM index and Niño3.4, and SOI are shown.

663